pp 141–162. © Royal Aeronautical Society 2016
doi: 10.1017/aer.2016.112

The efficiency analysis of high-altitude propeller based on vortex lattice lifting line theory

Xue-ke Zheng
zxk2046@sjtu.edu.cn

Xiao-liang Wang, Zhen-jin Cheng and Ding Han
Shanghai Jiao Tong University
Shanghai
China

ABSTRACT

In this paper, we proposed a simple approach to analyse the efficiency and propulsive characteristics of the high-altitude propeller in accordance to the Vortex Lattice Lifting line Method (VLM) theory, which is commonly used in preliminary design and parametric studies of propeller propulsion. The Computational Fluid Dynamics (CFD) method was used to obtain aerofoil aerodynamic data. The optimal pitch angle and propeller blade chord length (along the radial direction) can be calculated using the information from the database. The propeller wake model sees helical slipstreams applied to both lightly and moderately loaded propellers. The proposed method is capable of identifying the optimal efficiency through varying the number of propeller blades, radius and the rotational speed. The relationship between the optimal efficiency and design parameters is then established. This method was verified using CFD calculations.

Keywords: High-altitude propeller; optimal efficiency; Vortex Lattice Lifting line Method; propeller wake model

Received 21 February 2016; revised 10 September 2016; accepted 12 September 2016; first published online 22 November 2016.

https://doi.org/10.1017/aer.2016.112 Published online by Cambridge University Press

NOMENCLATURE

T	actual thrust of propeller
T_r	required thrust of propeller
V_s	horizontal flight speed of aircraft
Q	torque of propeller
ρ	air density
Z	number of blades
C_L	lift coefficient
C_D	drag coefficient
c	aerofoil chord length (m)
Γ	concentrate circulation
V^*	total inflow speed (m/s)
V_a	axial inflow velocity (m/s)
V_t	tangential inflow velocity (m/s)
u_a^*	induced axial velocity (m/s)
u_t^*	induced tangential velocity (m/s)
λ	Lagrange multiplier
KT	thrust coefficient based on blade tip speed
KQ	torque coefficient based on blade tip speed
Js	advance ratio
η	propeller efficiency (%)
ω	propeller angular velocity (rad/s)
N	propeller revolutions per minute (RPM)
R	propeller radius (m)
E_A	expanded area
E_o	disk area

1.0 INTRODUCTION

In recent years, the interest in stratospheric aircrafts has been increased considerably. Their long endurance, low energy consumption and high security make stratospheric aircrafts attractive for both military and civilian applications[1,2]. Propellers are widely used on aircrafts as a source of thrust[3,4]. The increased propulsion efficiency of the propeller is of great importance in aviation to reduce energy consumption and improve cruising periods. Although flight performance can be improved through the implementation of solar cells on the deck of the aircraft, it is still limited in the absence of sunlight. Significant propulsive performance improvements of propellers can be achieved through the optimization design due to the flight environment where the air density is much lower and the advance velocity of aircraft is extremely slow (about 10–30 m/s), which makes it a big challenge to design efficient propeller propulsions for stratospheric aircrafts[5]. Hence, the focus on improving the propulsive efficiency is a top priority.

There are two main propeller geometrical adjustments that could be made to improve the propeller performance[6]. Firstly, different aerofoil cross-sectional shapes will affect the lift coefficients at different altitudes, affecting the propeller efficiencies under different conditions[7,8]. Secondly, the variation of blade pitch angles and chord lengths will also alter the propulsive efficiency[9]. The VLM method[10,11] has been widely used in the design

https://doi.org/10.1017/aer.2016.112 Published online by Cambridge University Press

process of propellers for many years. It is capable of calculating the prime efficiency of an air propeller given wings with high aspect ratios. Coney[11] suggested an algorithm to determine the optimal radial distributions of circulation for propellers, which was incorporated into the propeller wake model for lightly to moderately loaded propellers. Epps et al[12] implemented Coney's generalised propeller optimiser and created an off-design analysis routine to predict the performance curve for a given propeller design. Epps[13] corrected the classical wake model used on moderately loaded propellers and identified a new wake model representing each panel as a constant-pitch vortex sheet. However, the methods mentioned above did not consider the aerodynamic properties of the aerofoil, such as the Reynolds number and Mach number at radial locations. These properties should be taken into consideration for high-altitude propellers.

The focus of this paper is a novel method based on Coney's optimiser[11] to optimise the blade chord and pitch distributions and obtain the desired circulation at the angle-of-attack where the aerofoil has a maximum lift-drag ratio. The pitch is calculated by the both values of inflow and desired angles-of-attack. The chord is also optimised by using the appropriate circulation, total inflow speed determined by Coney's method, and a proper lift coefficient where the lift-drag ratio is maximum. This approach results in a higher efficiency than prescribing chord arbitrarily. Furthermore, the effects of the Reynolds and Mach numbers, coupled with the aerofoil aerodynamic data from the CFD method, will be presented in this paper. The information will provide the ideal propeller characteristics with results close enough to CFD methods. The relation between the optimal efficiency and the design parameters of the propellers are obtainable. The design parameters include the number of blades, blade radius and rotation speed.

The paper is organised into five main sections. In Section 2, the algorithm for the propeller optimiser will be described, followed by the analysis of the aerodynamic characteristics of the S1223 aerofoil in Section 3. After which, the validation of the used method using the CFD method will be described in Section 4 and the analysis of the optimum efficiency and design parameters of propellers will be analysed in Section 5. Lastly, we will draw conclusions on the computational methods and propeller characteristics at high altitude.

2.0 THE IMPROVED ALGORITHM OF PROPELLER OPTIMISER

The relative velocity and forces on the propeller aerofoil are shown on the basis of VLM in Fig. 1, where ωr is the relative velocity of propeller and V_t, V_a and V_0 are the tangential, axial and composite inflow velocity, respectively. During the course of the propeller optimization design, the tangential inflow velocity was assumed to be negligible. u_t^* and u_a^* are the tangential and axial induced velocity, respectively, which can be calculated using tangential and axial induced factors $\bar{u}_t^*(m, i)$, $\bar{u}_a^*(m, i)$, $m, i = 1 \sim M$[14]. V^* is the composite velocity which takes into consideration the induced velocity. ϑ is the pitch angle, α is the angle-of-attack of the aerofoil. β is the aerodynamic pitch angle caused by V_t and V_a • β_i is the aerodynamic pitch angle that is a function of induced velocity. F_i, F_v and F are the inviscid lift force, viscous force and composite force, respectively. $T_{(i)}$ and $D_{(i)}$ are the actual thrust and drag of blade aerofoil.

The propeller has Z blades. Each blade was divided into M segments ($M = 15$)[12]. The concentrate circulation $\Gamma_{(i)}$ on each segment is a key variable that needs to be optimised.

https://doi.org/10.1017/aer.2016.112 Published online by Cambridge University Press

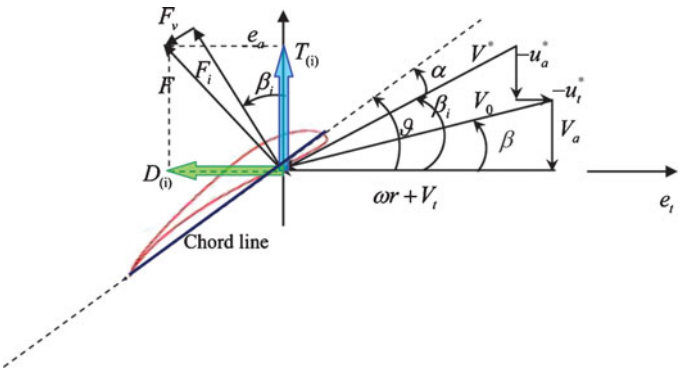


Figure 1. (Colour online) Velocity, angle and force diagram of blade aerofoil.

Assuming the Z blades are identical, the total thrust T and torque Q on the propeller[12] are:

$$T = Z\int_{r_h}^{R}[F_i\cos\beta_i - F_v\sin\beta_i]dr, \quad \ldots(1)$$

$$Q = Z\int_{r_h}^{R}[F_i\sin\beta_i + F_v\cos\beta_i]rdr \quad \ldots(2)$$

Based on the trigonometric relations between β_i and the blade, the total thrust and torque on the propeller are:

$$T = \rho Z\sum_{i=1}^{M}\{[\omega r + V_t + u_{t(i)}{}^*]\cdot\Gamma_{(i)} - \frac{1}{2}V_{(i)}{}^*C_{D(i)}c_{(i)}[V_a + u_{a(i)}{}^*]\}\Delta r, \quad \ldots(3)$$

$$Q = \rho Z\sum_{i=1}^{M}\{[V_a + u_{a(i)}{}^*]\cdot\Gamma_{(i)} + \frac{1}{2}V_{(i)}{}^*C_{D(i)}c_{(i)}[\omega r + V_t + u_{t(i)}{}^*]\}r\Delta r, \quad \ldots(4)$$

where u_a^* and u_t^* are obtained by combing circulation $\Gamma_{(i)}$ with tangential and axial velocity induced factors $\bar{u}_t^*\&\bar{u}_a^*$ in wake alignment model[13]. u_a^* and u_t^* are formulated as:

$$u_{a(m)}^* = \sum_{i=1}^{M}\Gamma(i)\bar{u}_a^*(m,i), \quad \ldots(5)$$

$$u_{t(m)}^* = \sum_{i=1}^{M}\Gamma(i)\bar{u}_t^*(m,i) \quad \ldots(6)$$

The propulsive efficiency of propeller can be written as:

$$\eta = \frac{TV_s}{Q\omega}, \quad \ldots(7)$$

https://doi.org/10.1017/aer.2016.112 Published online by Cambridge University Press

where V_s is the flight speed of aircraft and ω is the angular velocity of propeller rotation. The flight speed of aircraft V_s is assumed to be equivalent to the axial inflow velocity V_a.

To obtain the maximum efficiency η, Coney[11] employs the method of Lagrange multiplier from variational calculus. He forms an auxiliary function:

$$H = Q + \lambda(T - T_r) \quad \ldots(8)$$

If, when $T = T_r$, min H = min Q.

For the minimum H, the derivatives with respect to the unknowns are assumed negligible.

$$\frac{\partial H}{\partial \Gamma_{(i)}} = 0 \quad \text{for } i = 1...M, \quad \ldots(9)$$

$$\frac{\partial H}{\partial \lambda} = 0 \quad \ldots(10)$$

From Equations (9) and (10), we can obtain a system of M+1 nonlinear equations for M+1 unknown variables. For solving the optimised circulation distribution and flow parameters, these systems can be linearised by freezing flow parameters $\{u_a^*, u_t^*, \bar{u}_a^*, \bar{u}_t^*, V^*, \frac{\partial V^*}{\partial T}, \lambda\}$. More details can be found in Coney[11] and Epps et al[12].

Based on the required thrust of the propeller, the number of blades, the propeller radius, the rotation speed, and the airspeed of aircraft, the ideal circulation distribution can be obtained using Coney's optimization method.

$c_{(i)}$ can be optimised by making every aerofoil section under the condition of maximum lift-drag ratio $(L/D)_{\max}$. $c_{(i)}$ is deduced as:

$$c_{(i)} = \frac{2\Gamma_{(i)}}{V_{(i)}^* \cdot C_{L(i)_(L/D)_{\max}}} \quad \ldots(11)$$

Substituting Equation (11) and $C_{D(i)_(L/D)_{\max}}$ into Equations (3) and (4) and rewriting them:

$$T = \rho Z \sum_{i=1}^{M} (\omega r + V_t + u_{t(i)}^* - \frac{V_a + u_{a(i)}^*}{(L/D)_{\max}}) \cdot \Gamma_{(i)} \Delta r, \quad \ldots(12)$$

$$Q = \rho Z \sum_{i=1}^{M} (V_a + u_{a(i)}^* + \frac{\omega r + V_t + u_{t(i)}^*}{(L/D)_{\max}}) \cdot \Gamma_{(i)} r \Delta r \quad \ldots(13)$$

According to Equations (12) and (13), the systems can be linearised by freezing flow parameters $\{u_a^*, u_t^*, \bar{u}_a^*, \bar{u}_t^*, C_{L(i)_(L/D)_{\max}}, C_{D(i)_(L/D)_{\max}}, (L/D)_{\max}, \lambda\}$.

Before updating $(L/D)_{\max}$, $c_{(i)}$ should be computed by using Equation (14):

$$c_{(i)} = \frac{2\Gamma_{(i)}}{V_{(i)}^* \cdot \hat{C}_{L(i)_(L/D)_{\max}}}, \quad \ldots(14)$$

where $V_{(i)}^*$ can computed as:

$$V_{(i)}^* = \sqrt{(V_a + u_{a(i)}^*)^2 + (\omega r + V_t + u_{t(i)}^*)} \quad \ldots(15)$$

https://doi.org/10.1017/aer.2016.112 Published online by Cambridge University Press

Note that $\hat{C}_{L(i)_(L/D)_{\max}}$ in equation (14) is a frozen value. The Reynolds number $\mathrm{Re}(c_{(i)})$ and the Mach number $\mathrm{Ma}(c_{(i)})$ can be attained by applying $c_{(i)}$ into Equation (14):

$$\mathrm{Re}_{(i)} = \frac{\rho \cdot c_{(i)} \cdot V^*_{(i)}}{\mu}, \quad \ldots(16)$$

$$\mathrm{Ma}_{(i)} = \frac{V^*_{(i)}}{c}, \quad \ldots(17)$$

where ρ is air density, μ is dynamic viscosity and c is local air velocity.

The Reynolds number and Mach number obtained from Equations (16) and (17), along with aerodynamic properties of the aerofoil, will determine a new maximum lift-drag ratio, $(L/D)_{\max}$. (The aerodynamic properties will be discussed in Section 3.) New values of the lift coefficient, $C_{L(i)_(L/D)_{\max}}$, drag coefficient, $C_{D(i)_(L/D)_{\max}}$, and the angle-of-attack at each aerofoil section, $\alpha_{(i)_(L/D)_{\max}}$, will also be updated according to the new maximum lift-drag ratio.

As is shown in Fig. 1, β_i can be determined by:

$$\beta_{i(i)} = \arctan \frac{V_a + u^*_a}{\omega r + V_t + u^*_t} \quad \ldots(18)$$

$\vartheta_{(i)}$ is computed as:

$$\vartheta_{(i)} = \alpha_{(i)_(L/D)_{\max}} + \beta_{i(i)} \quad \ldots(19)$$

The flow chart for optimum propeller design is shown in Fig. 2.

3.0 THE AERODYNAMIC CHARACTERISTICS OF S1223 AEROFOIL

For the high-aspect-ratio blade, the aerodynamic characteristics of a two dimension aerofoil is very important for the three dimension propulsive performance. In Tang et al[5], the Reynolds numbers of high-altitude propellers range from 10^5 to 10^6, which may be defined as the lower range of Reynolds numbers. Aerofoil S1223 has a Reynolds number that falls within the defined low range[8]. Therefore, this aerofoil was chosen for this paper. The thrust of the propeller at a high altitude is small compared to that just above ground, reducing the structural requirements of the propeller. Furthermore, Tang has performed a wind tunnel experiment for high-altitude propellers using aerofoil S1223. Thus, the structural integrity of the aerofoil is not a main concern in the design of high-altitude propellers. The contour of aerofoil S1223 is shown in Fig. 3.

The aerodynamic characteristics of aerofoil S1223 fall in the regions of Reynolds number ($\mathrm{Re} = 3{,}000 \sim 2.0 \times 10^7$), Mach number ($\mathrm{Ma} = 0.05 \sim 0.9$) and angel of aerofoil (alpha = 0∼16º). These properties will be used to obtain the accurate chord length and pitch angle distribution of propeller blades. The aerodynamic characteristics were calculated by CFD method (FLUENT). The mesh of aerofoil S1223 is shown in Fig. 4. The obtained aerodynamic data is assumed to be the database in the propeller optimization design.

https://doi.org/10.1017/aer.2016.112 Published online by Cambridge University Press

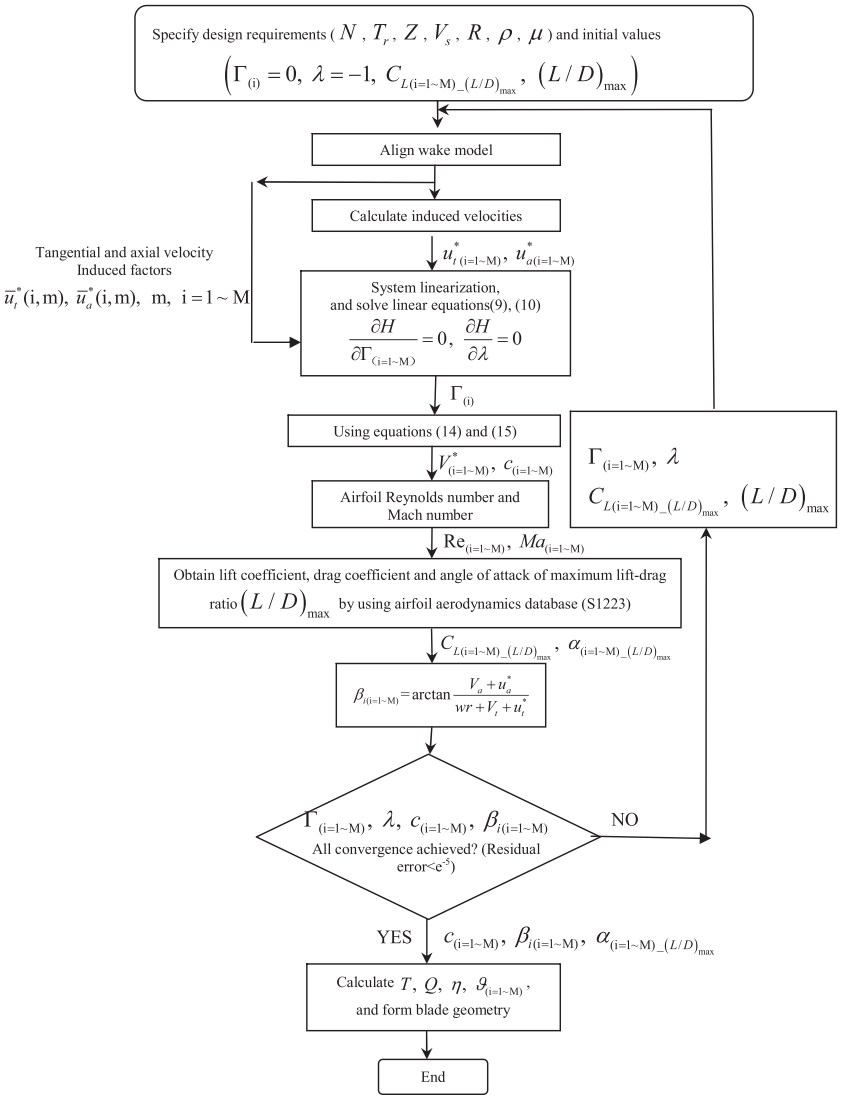


Figure 2. Flow chart for optimum propeller design.

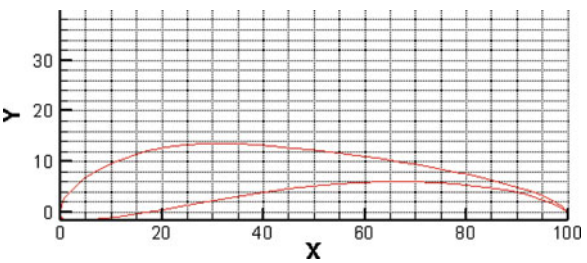


Figure 3. (Colour online) Contour of aerofoil S1223.

https://doi.org/10.1017/aer.2016.112 Published online by Cambridge University Press

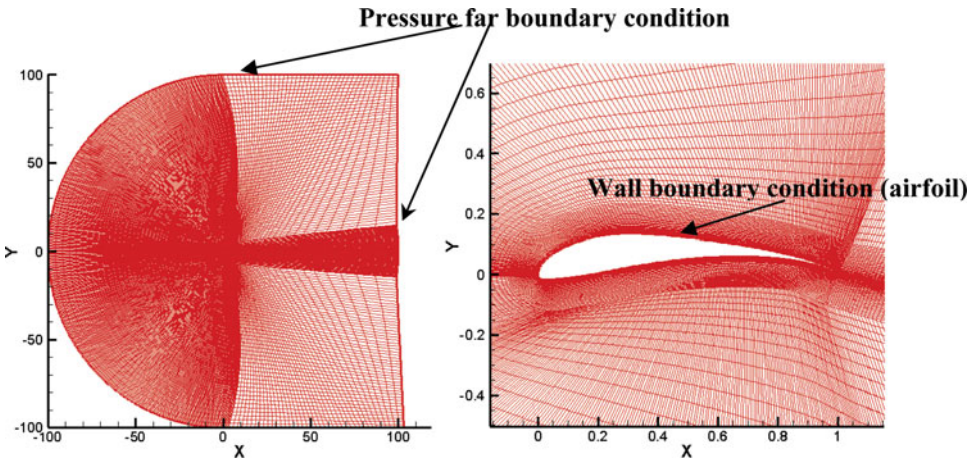
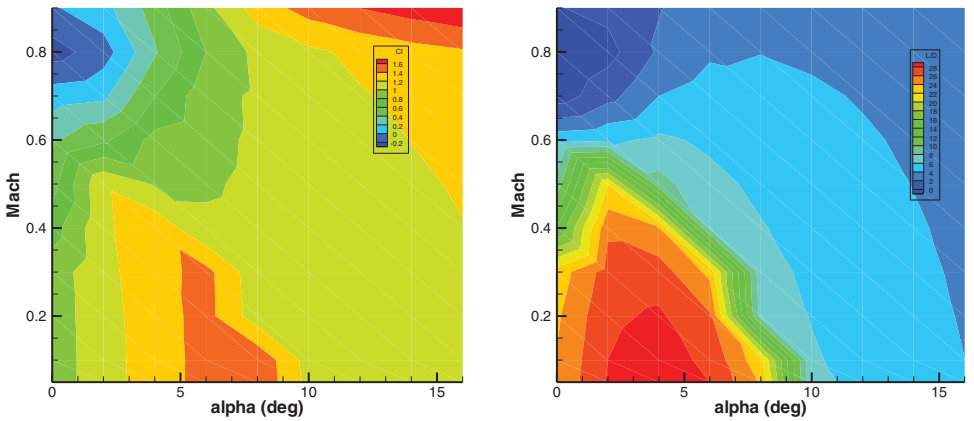


Figure 4. (Colour online) The boundary condition and mesh used in FLUENT.



(lift coefficient) (lift-drag ratio)

Figure 5. (Colour online) The lift coefficient and lift-drag ratio on Re = 30,000.

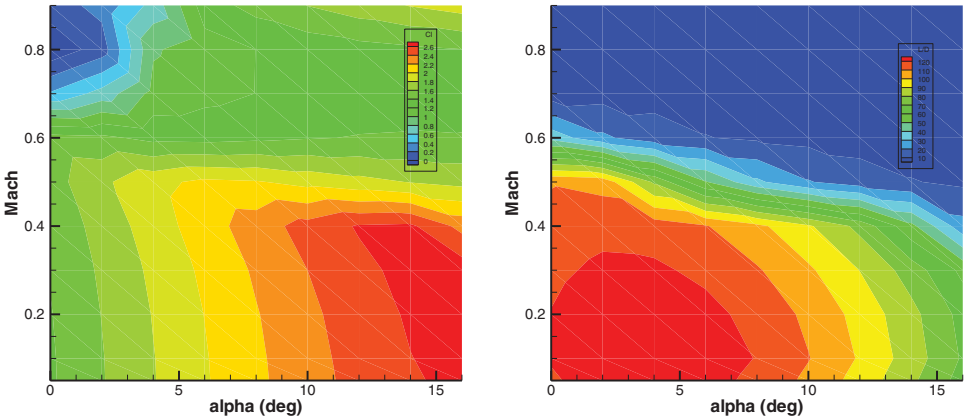
The calculation conditions of aerodynamic data are:

Mach number: 0.05, 0.1 ~ 0.9 (interval 0.1).
Reynolds number: 3×10^4, 6×10^4, 1.2×10^5, 1.8×10^5, 4.8×10^5, 9.6×10^5, 1.5×10^6, 5.5×10^6, 1.0×10^7, 2.0×10^7.

The lift coefficient and lift-drag ratio on Re = 30,000 and 2.0×10^7 are shown in Figs 5 and 6.

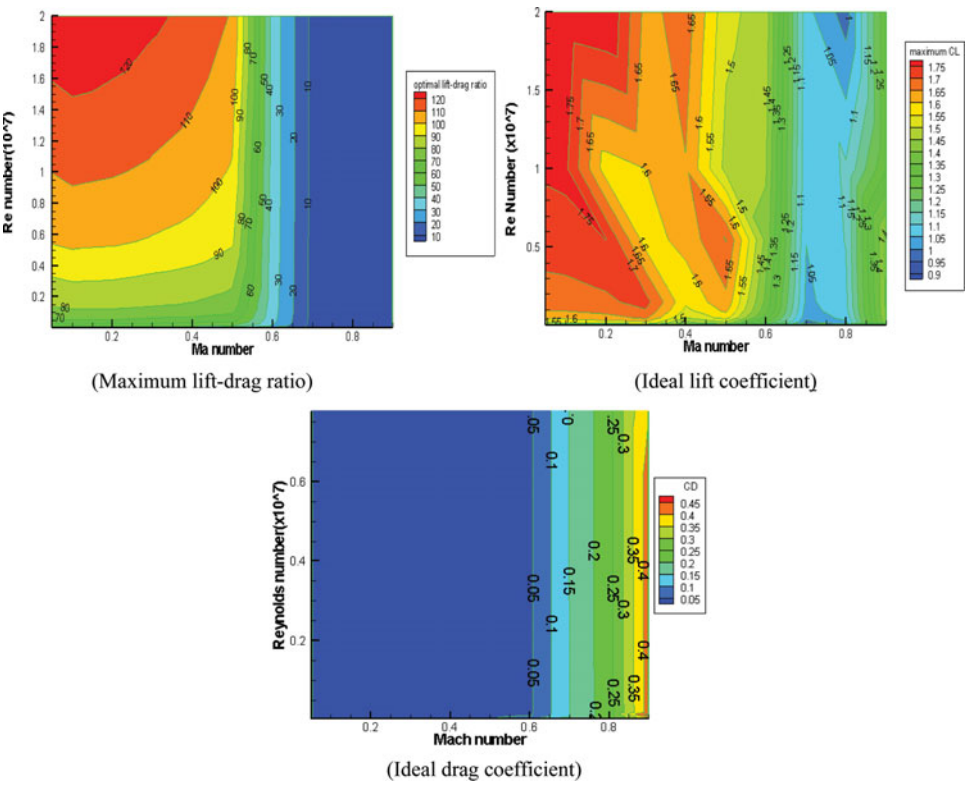
The maximum lift-drag ratio and ideal lift coefficient of maximum lift-drag ratio with variation of Reynolds number and Mach number are shown in Fig. 7. It is clearly seen that the maximum lift-drag ratio and ideal lift coefficient of maximum lift-drag ratio decline as the Mach number increases, especially when it exceeds the critical Mach of aerofoil S1223. The critical Mach number can be derived from Fig. 7, which shows that the value of optimal drag coefficient is increased dramatically when the Mach number exceeds 0.6. Also, the estimation method for the critical Mach of aerofoil can be found in Tang[15].

https://doi.org/10.1017/aer.2016.112 Published online by Cambridge University Press



(lift coefficient) (lift-drag ratio)

Figure 6. (Colour online) The lift coefficient and lift-drag ratio on $Re = 2.0 \times 10^7$.



(Maximum lift-drag ratio) (Ideal lift coefficient)

(Ideal drag coefficient)

Figure 7. (Colour online) The optimal lift-drag ratio, ideal lift coefficient and ideal drag coefficient of aerofoil S1223 under conditions of different Reynolds numbers and Mach numbers.

https://doi.org/10.1017/aer.2016.112 Published online by Cambridge University Press

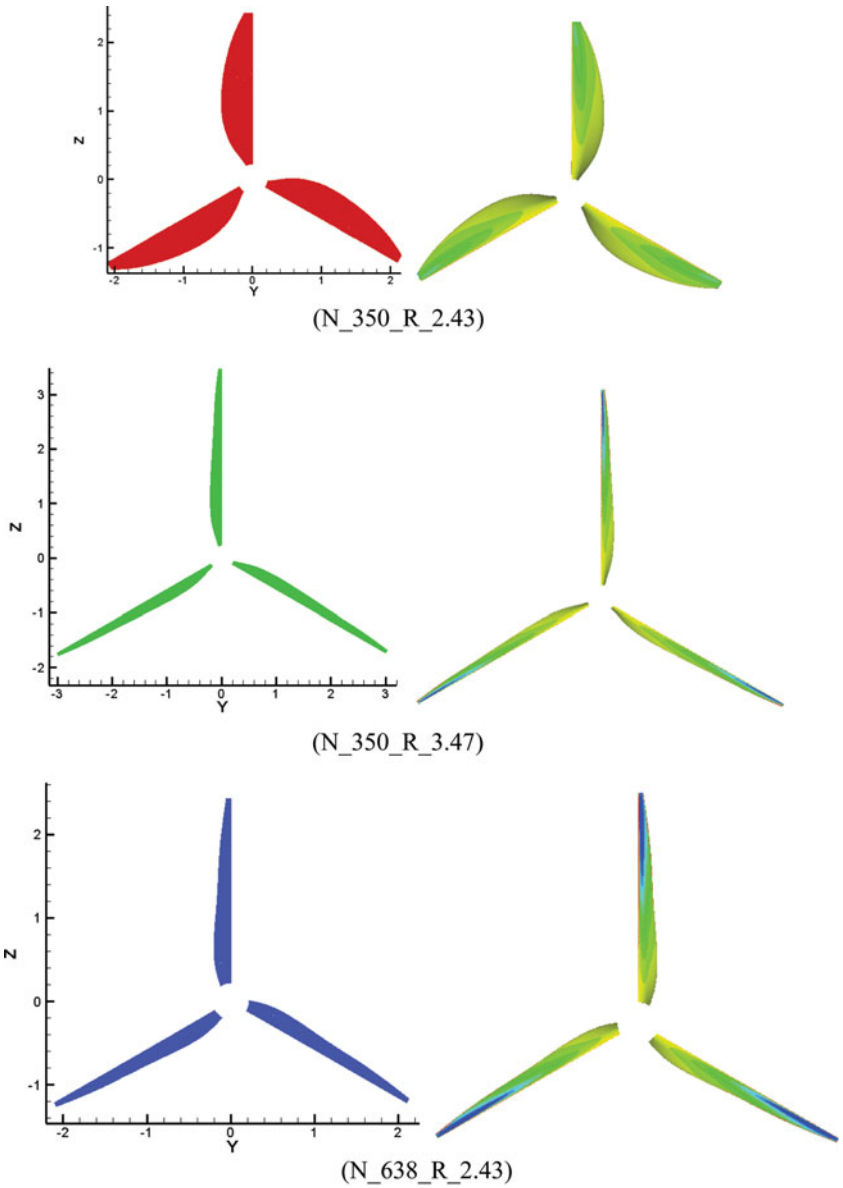


Figure 8. (Colour online) The propeller shape and pressure coefficient distribution of three propellers.

4.0 VALIDATION OF THE PROPELLER OPTIMIZATION METHOD

The propeller performances were analysed using the vortex lattice lifting line method (VLM) theory and the accurate aerofoil aerodynamic data was obtained by the CFD method. Moreover, the chord length and pitch angle distribution were gained through the maximum lift-drag ratio of the aerofoil.

https://doi.org/10.1017/aer.2016.112 Published online by Cambridge University Press

Table 1
The efficiencies of three propellers using different methods

Name	F(N) (VLM)	M(N.m) (VLM)	Efficiency (VLM)	F(N) (FLUENT)	M(N.m) (FLUENT)	Efficiency (FLUENT)	Efficiency with finite aspect ratio correction
N_350_R_2.43	484.0	437.98	60.3%	424.5	389.4	59.48%	59.29%
N_350_R_3.47	484.0	363.28	72.7%	495.2	409.3	66.0%	69.21%
N_638_R_2.43	484.0	226.74	63.9%	488.2	258	56.63%	58.4%

To verify the capability of the improved method, three different propellers were calculated using the CFD method. The three propellers were obtained using the optimised method. The design conditions of propeller are:

Flight speed of aircraft: $V_s = 20$ m/s.

Required thrust of propeller: $T_r = 484$ N.

The numerical method used in this paper is the FLUENT 6.3.26 steady Reynolds-averaged Navieer-Stokes solver[16]. The control equations were solved using density-based solver, single precision, second order in space. The flux type is Roe-FDS. The courant number is 5. A one-equation Spalart-Allmaras (S-A) model[17] was used.

The fluid boundary is 50 times longer than blade length. The fluid mesh is unstructured mesh (the cell number is about 2.34 million). The fluid field was divided into an outer region and an inner region. The motion of the propeller uses the moving reference frame on the inner region, which attaches with the propeller. The boundaries are the pressure far-boundary condition.

Comparing the results obtained from the CFD method and the improved VLM method, we can see that the error of the propeller is about 6%. There is no standard model for high-altitude propellers[18]. The error from the VLM can be validated using the CFD method. The CFD results are assumed to have small errors. The VLM error of 6% is relative to the CFD results. In addition, an error of 6% is reasonable since the error using the JBLADE method[18] exceeds 10%. The VLM has been verified using 4119 and 4381 propellers by Epps and Kimball[13].

As for propeller blades, they have a finite span and the performance of those finite-span blades differ significantly from the performance of the corresponding two-dimensional aerofoils. The finite aspect ratio correction[13,19] is:

$$C_{L\alpha}^{3D} = \frac{C_{L\alpha}^{2D}}{1 + C_{L\alpha}^{2D}/(\pi e AR)} \quad \ldots (20)$$

where $C_{L\alpha}^{3D}$ is the lift slope after the correction (3D aerofoil), $C_{L\alpha}^{2D}$ is the lift slope for an infinite blade (2D aerofoil), e is a span efficiency factor and AR is the aspect ratio of the blade. As is shown in Table 1, the finite aspect ratio correction would improve the accuracy of the propeller geometry and reduce the differences between the CFD and VLM results.

https://doi.org/10.1017/aer.2016.112 Published online by Cambridge University Press

Table 2
The efficiencies of three propellers using different methods

Name	F(N) (VLM) Original	M(N.m) (VLM) Original	Efficiency (VLM) Original	Lift -drag ratio Original (75% radial position)	F(N) (VLM) Improved	M(N.m) (VLM) Improved	Efficiency (VLM) Improved(%)	Lift -drag ratio Improved (75% radial position)
N_350_R_2.43	484	431.49	59.2	39.60	484	437.98	60.3	56.37
N_350_R_3.0	484	402.43	63.5	20.19	484	368	69.5	48.43
N_350_R_3.47	484	419.81	60.9	12.16	484	363.28	72.7	42.71
N_638_R_2.43	484	252.80	55.5	15.11	484	226.74	63.9	43.78

Table 3
Efficiency performances of specified propellers under different maximum lift-drag ratio situations

N = 350 rpm	R = 3.5 m	L/D	Efficiency
		10	55.3%
		15	60.7%
		20	63.7%
		25	65.6%
		30	67.0%
		35	68.0%
		40	68.7%
		45	69.3%

The improved VLM method can obtain the characteristics of different propellers. For the propulsion of aircraft, it is desirable to use low disk loading propellers (i.e., a lightly and moderately loaded propeller) that can obtain greater efficiency[3]. The propeller wake model of the improved VLM method is a regular helical slipstream. This wake model can be applied to lightly and moderately loaded propellers effectively. The performances using the original and improved methods are presented in Table 2. It is shown that the efficiency derived from the improved method is higher than that derived from the original method. As is shown in Table 3, if we fix the maximum lift-drag ratio $(L/D)_{\max}$ term in Equations (12), (13) and prevent it from updating in the iterative process shown in Fig. 2, the efficiency performance is better with the increasing value of maximum lift-drag ratio, which means the maximum lift-drag ratio indeed contributes to the performance of the improved method. Lift-drag ratios at 75% radial position of the original and improved methods are also shown in Table 2. In the original method, the chord distribution is determined in advance. The chord distribution which has been given in Liu et al[4] is shown in Fig. 9. In the improved method, the chord distributions are optimised during the process of the algorithm presented in Fig. 2 and are also shown in Fig. 9.

https://doi.org/10.1017/aer.2016.112 Published online by Cambridge University Press

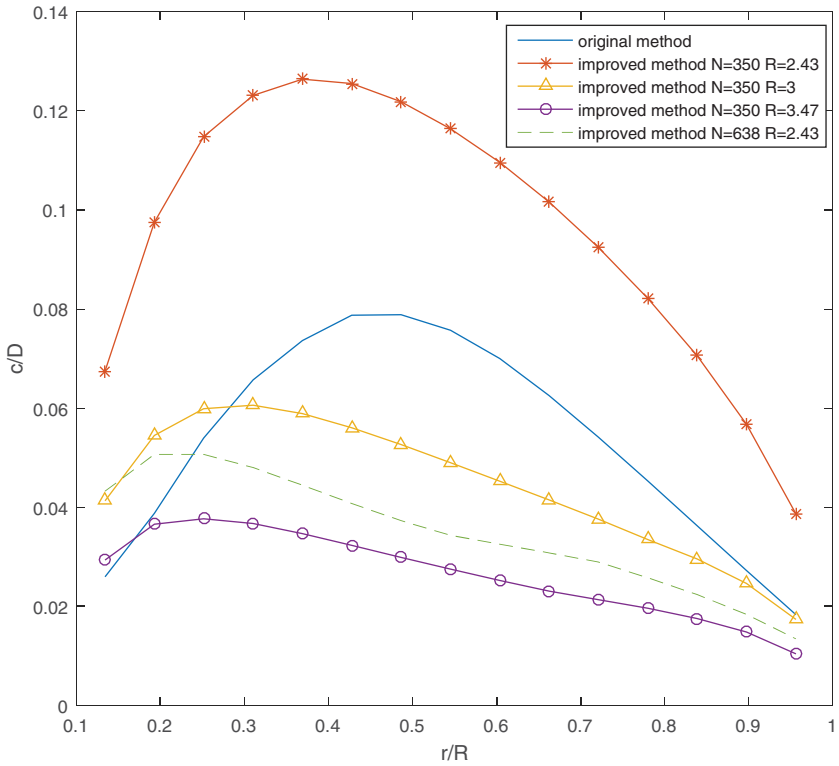


Figure 9. (Colour online) The chord distribution of propellers in the original and improved method.

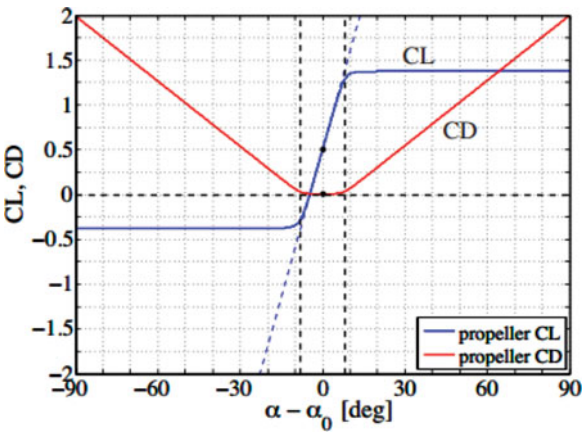
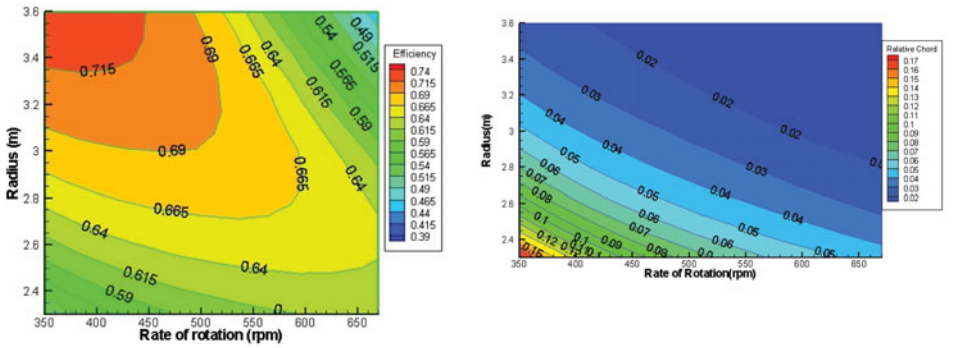


Figure 10. (Colour online) Lift and drag coefficient versus net angle-of-attack.

https://doi.org/10.1017/aer.2016.112 Published online by Cambridge University Press



(a) Optimal efficiency (b) Relative chord length (c/D) at 75% radial position

Figure 11. (Colour online) Z = 2, N = 350-670, R = 2.3–3.6.

The lift and drag coefficient computed in the original method are shown in Fig. 10 and given by these equations:

$$C_L = C_{L0} + \frac{dC_L}{d\alpha}\Delta\alpha - \frac{dC_L}{d\alpha}(\Delta\alpha - \Delta\alpha_{stall}) \cdot F(\Delta\alpha - \Delta\alpha_{stall}) + \frac{dC_L}{d\alpha}(-\Delta\alpha - \Delta\alpha_{stall}) \cdot F(-\Delta\alpha - \Delta\alpha_{stall}) \quad \ldots(21)$$

$$C_D = C_{D0} + A \cdot (\Delta\alpha - \Delta\alpha_{stall}) \cdot F(\Delta\alpha - \Delta\alpha_{stall}) + A \cdot (-\Delta\alpha - \Delta\alpha_{stall}) \cdot F(-\Delta\alpha - \Delta\alpha_{stall}) - 2A \cdot (-\Delta\alpha_{stall}) \cdot F(-\Delta\alpha_{stall}) \quad \ldots(22)$$

where C_{L0}, $C_{D0}$and α_0 are ideal values of C_L, C_D and α, respectively. $F(x)$ is an auxiliary function, the net angle-of-attack $\Delta\alpha = \alpha - \alpha_0$, $\Delta\alpha_{stall}$ is the stall angle, A is the drag coefficient post-stall slope, and $\frac{dC_L}{d\alpha}$ is the lift curve slope, More details about the calculation of the lift and drag coefficient in the original method can be found in Epps and Kimball[13].

By using Equation (11), the lift coefficient can be deduced as:

$$C_{L(i)} = \frac{2\Gamma_{(i)}}{V^*_{(i)} \cdot c_{(i)}} \quad \ldots(23)$$

Thus, the drag coefficient and the angle-of-attack during the process of the optimisation in the original method are determined by using Equations (21) and (22). The optimization algorithm in the original strategy can be obtained from Coney[11].

5.0 EFFICIENCY OPTIMISED BY RATE OF ROTATION, PROPELLER RADIUS AND BLADE NUMBER

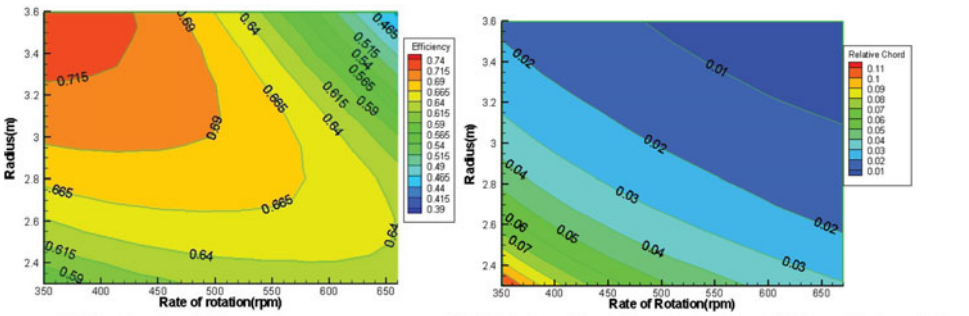
In general, the length of stratosphere aircraft is about 150–200 m. The volume of the aircraft hull is about 300,000 m^3. In this paper, we used the thrust needed on a stratosphere aircraft as the design conditions of a high-altitude propeller.

In this section, the optimum efficiency of propellers under the condition of different rate of rotation, propeller radius and blade number are analysed using the improved VLM method. The optimised characteristics, including efficiency and relative chord length with different parameters, are presented in Figs 11-13. It is shown that the chord length is decreased with the

https://doi.org/10.1017/aer.2016.112 Published online by Cambridge University Press

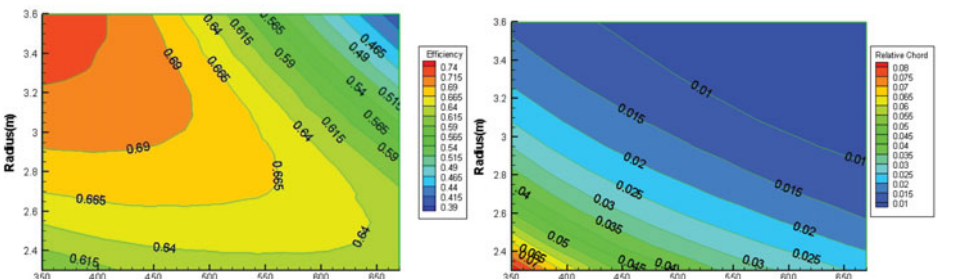
Table 4
The size of stratosphere aircraft and needed thrust parameter

Length of aircraft	**160 m**	**Needed thrust**	**2,420.956 N**
Volume of aircraft	304,860 m^3	Number of propellers	5
Drag coefficient	0.03	Required thrust of each propeller	**484 N**
Flight velocity	**20 m/s**	Air density & dynamic viscosity	0.0889 kg/m3 1.42161e-005 kg/(m.s)



(a) Optimal efficiency (b) Relative chord length (c/D) at 75% radial position

Figure 12. (Colour online) Z = 3, N = 350–670, R = 2.3–3.6.



(a) Optimal efficiency (b) Relative chord length (c/D) at 75% radial position

Figure 13. (Colour online) Z = 4, N = 350–670, R = 2.3–3.6.

increasing number of blades at the specified thrust requirement. The propellers' parameters with the maximum efficiency in Fig. 12 are shown in Table 5.

From the results shown in Figs 11-13, we can see that, at certain blade numbers and rates of rotation, the optimum efficiency has maximal value with the variation of the radius. Also, the optimum efficiency has maximal value when blade number and rate of rotation are certain. In design condition, the optimum efficiency of rate of rotation number N = 510 rpm and radius R = 2.69 m at blade number Z = 3 is shown in Figs 14 and 15 respectively.

https://doi.org/10.1017/aer.2016.112 Published online by Cambridge University Press

Table 5
The propellers parameters with the maximum efficiency

Blade number	Blade radius (m)	Flight speed of aircraft (m/s)	Rotational speed (rpm)	Relative radius (r/R)	Chord distribution (c/D)	Torsional angle distribution (deg)	Efficiency
3	3.6	20	350	0.1340	0.0268	57.1367	73.48%
				0.1927	0.0329	46.9447	
				0.2515	0.0335	39.6397	
				0.3102	0.0323	34.2333	
				0.3689	0.0303	30.1446	
				0.4276	0.0281	26.9736	
				0.4863	0.0258	24.4573	
				0.5450	0.0237	22.4195	
				0.6037	0.0218	20.7396	
				0.6624	0.0200	19.2598	
				0.7211	0.0186	17.5530	
				0.7798	0.0172	16.0131	
				0.8385	0.0154	14.6073	
				0.8973	0.0130	13.4472	
				0.9560	0.0091	12.7633	

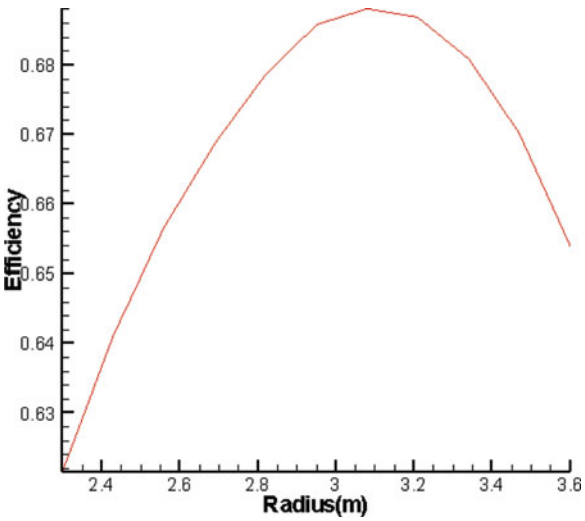


Figure 14. (Colour online) Rate of rotation number is 510 rpm.

The optimum efficiency differences between different blade numbers are shown in Figs 16-18 (a). As is shown in Figs 16-18 (b), the expanded area ratios are almost constant, which means blade area has no effect on efficiency in the comparative study. It is clearly seen that the optimum efficiency goes up with the increase of the blade number when the tip-speed

https://doi.org/10.1017/aer.2016.112 Published online by Cambridge University Press

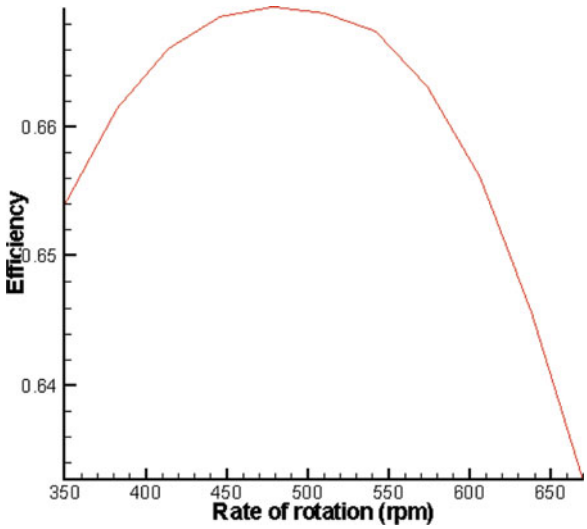


Figure 15. (Colour online) The radius of blade is 2.69 m.

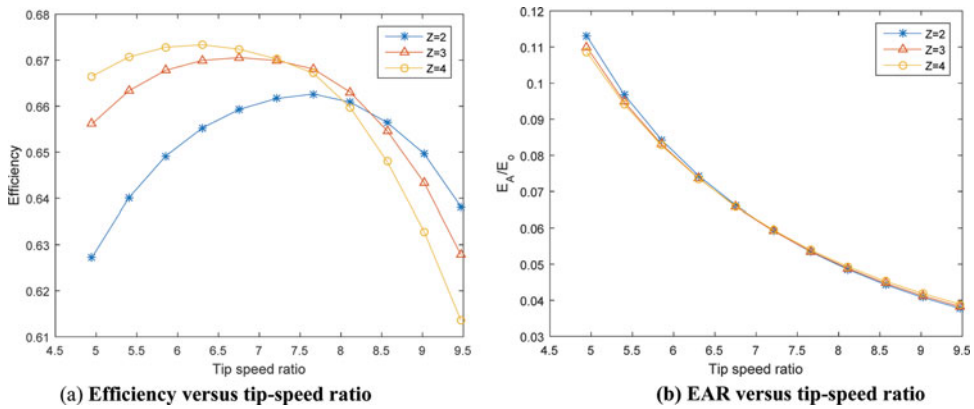
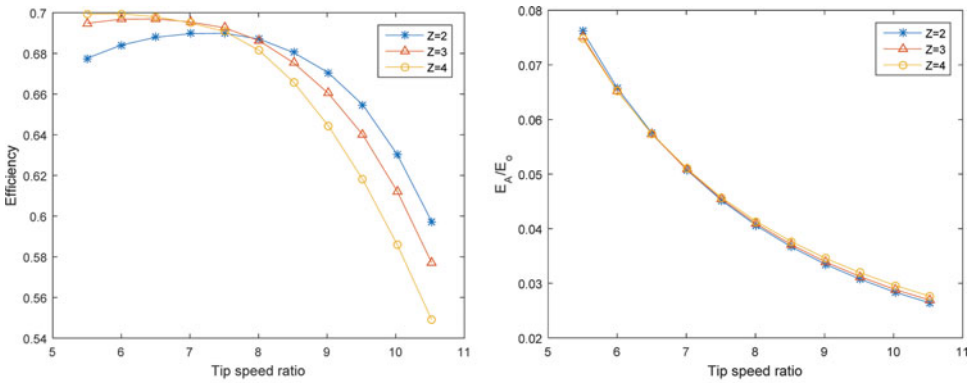


Figure 16. (Colour online) The design radius is R = 2.7 m.

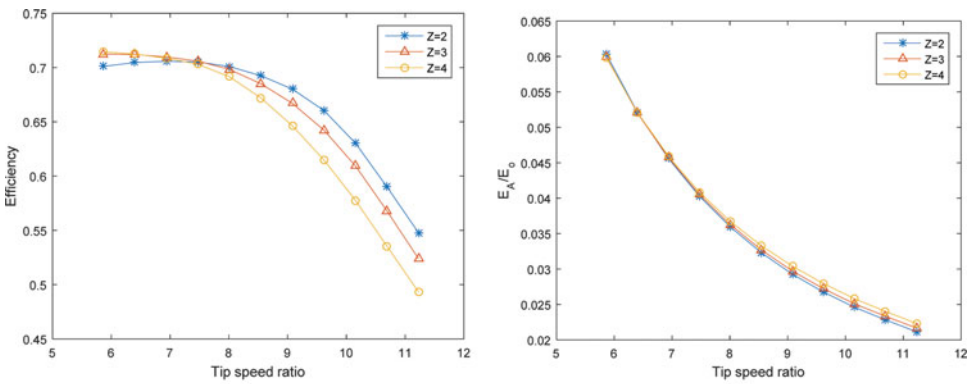
ratio is small, but as the tip-speed ratio increases, the result reverses. This is because as Z increases, blade-to-blade interaction induces performance decay and lowers the efficiency[20]. This is obvious when the advance ratio J is low and the rotation speed is relatively high. As in shown in Figs 19 and 20, when the propeller turns at a low speed, the orientation of the composite velocity V^* is distant from the plane of rotation, but as rotation speed increases, the composite velocity V^* "lies" in the plane of rotation. At a high rotation speed, if blades are too close, the strong interblade interaction is obvious, since the composite velocity V^* of the "back" blade is affected by the wake of the "forward" blade. The composite velocity V^* can flow between the blades but is affected by turbulence over the blades due to the wake. Also, viscous drag dominates at a very high rotation speed. These two factors reduce the efficiency at a high rotation speed. At a low rotation speed, the influence of blade-to-blade interaction

https://doi.org/10.1017/aer.2016.112 Published online by Cambridge University Press



(a) Efficiency versus tip-speed ratio (b) EAR versus tip-speed ratio

Figure 17. (Colour online) The design radius is R = 3 m.



(a) Efficiency versus tip-speed ratio (b) EAR versus tip-speed ratio

Figure 18. (Colour online) The design radius is R = 3.2 m.

is relatively small and negligible. The efficiency is then affected by other factors such as the circulation distribution, aerofoil characteristics and the number of blades.

6.0 CONCLUSIONS

The paper proposes an improved method to design high-altitude propellers based on an algorithm of propeller optimisation, which is a fast and accurate propeller design method. The method determines the optimum propeller chord lengths and pitch angle through considering the variation of Reynolds numbers and Mach numbers at radial locations which are sensitive on high-altitude propellers. It can be a useful tool to analyse the relations between optimum efficiency and design parameters of propellers. Through the analysis of optimum efficiency of propellers under the condition of different rates of rotation, propeller radius, and blade number, the obtained distribution results of optimum efficiency with parameters

https://doi.org/10.1017/aer.2016.112 Published online by Cambridge University Press

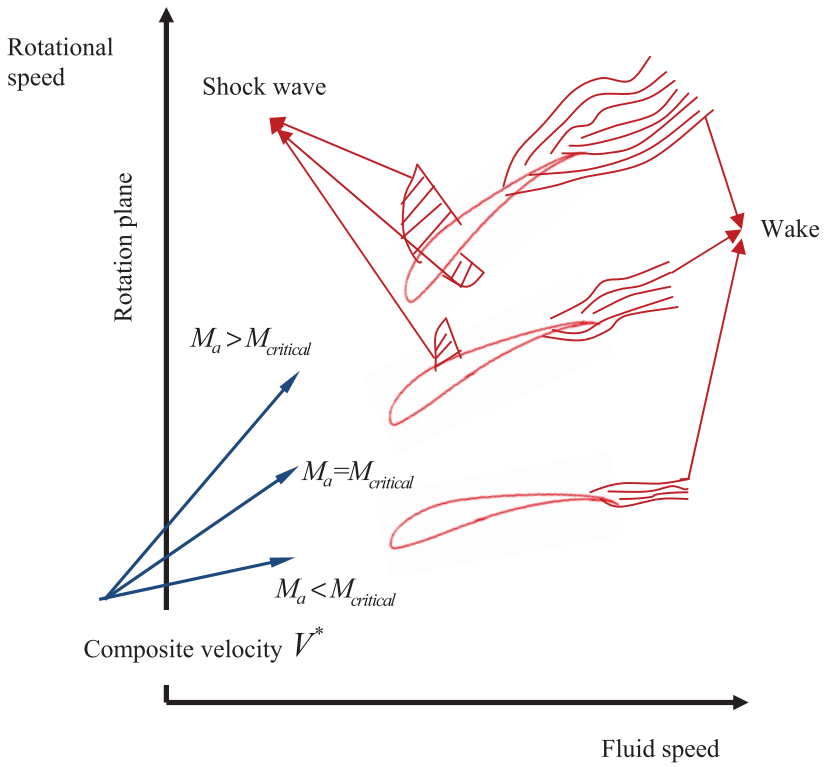


Figure 19. (Colour online) Aerofoil sections under different composite velocities[21].

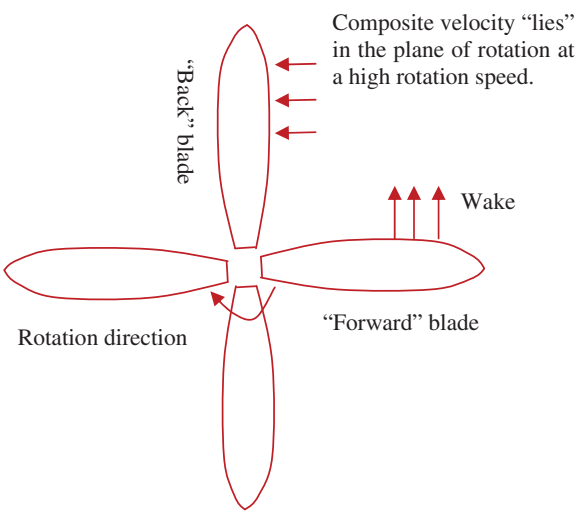


Figure 20. (Colour online) "Forward" and "back" blade.

https://doi.org/10.1017/aer.2016.112 Published online by Cambridge University Press

Table A1
Case: N_638_R_2.43 (VLM efficiency is 63.9%)

Name	F(N) (FLUENT)	M(N.m) (FLUENT)	Efficiency (FLUENT)	Cells number	Maximal Y+	
N_638_R_2.43	488.2	258	56.63%	1132751	310	Used in the paper
N_638_R_2.43	463.7	248.25	55.9%	1619657	60	
N_638_R_2.43	463.91	247.89	56.0%	3411083	30	

Table A2
The calculation conditions of DTMB 4119 propeller

Water density & dynamic viscosity	**998.0 kg/m^3, 0.001 kg/(m.s)**
Flow velocity	2.5389 m/s
Rotation speed	600 rpm
Diameter of propeller	0.3048 m
Free stream turbulence	1.6% of the freestream velocity

Table A3
Discretisation of DTMB 4119 propeller using CFD method

Pressure	**second order**
Momentum	second order upwind
Modified turbulent viscosity	second order upwind

can be used to select the high-altitude propellers in the initial design stage of a stratosphere aircraft.

APPENDIX A

The mesh used in this paper is refined and analysed. The results are shown in Table A1:

From the results, we can see that the mesh cell number and the Y+ (the boundary layer mesh) cannot affect the efficiency of the propeller considerably. The efficiency of the propeller is accurate when the mesh (cells number: 1132751, maximal Y+ = 310) is used in this paper. For verifying the accuracy of the CFD method, we can only find the experimental data of DTMB 4119 propeller[22]. The calculation conditions and discretisation of DTMB 4119 propeller when using CFD method is shown in Table A2 and Table A3. The CFD mesh (cell number: 2409890) of the DTMB4119 propeller is shown in Fig. A1.

We have used different meshes (such as the refined wake region mesh and the boundary layer mesh), but the results of the CFD are almost the same. The results are shown in the Table A4.

https://doi.org/10.1017/aer.2016.112 Published online by Cambridge University Press

Table A4
Comparison of the results of DTMB 4119 propeller using the CFD method and the experiment

Advance Ratio (J)	KT (CFD)	10KQ (CFD)	Efficiency (CFD)	KT (Experiment)	10KQ (Experiment)	Efficiency) (Experiment)	Discretisation
0.833	0.146023	0.31499	0.614	0.146	0.28	0.691	standard
0.833	0.140648	0.028757	0.648424	0.146	0.28	0.691	second order

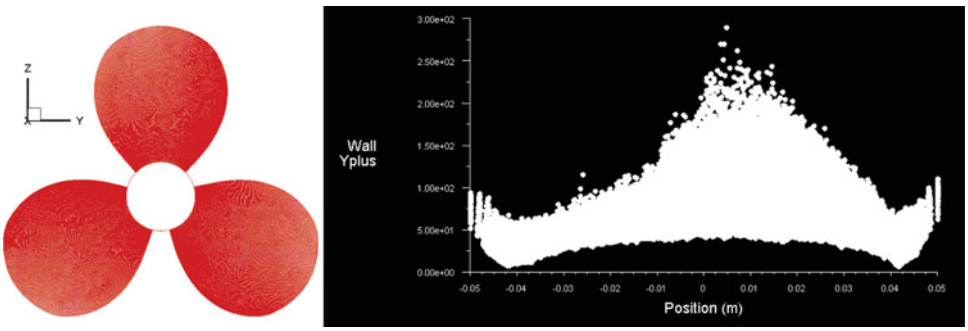


Figure A1. (Colour online) The CFD mesh of DTMB4119 propeller.

REFERENCES

1. COLOZZA, A. and DOLCE, J. Initial feasibility assessment of a high altitude long endurance airship. NASA CR-2203-212724, December 2003, National Aeronautics and Space Administration Washington, DC, US.
2. JAMISON, L., SOMMER, G.S. and PORCHE, I.R. High-altitude airships for the future force army, 2005, Rand Arroyo Center, Santa Monica, California, US.
3. ILIEVA, G., PÁSCOA, J., DUMAS, A. and TRANCOSSI, M. A critical review of propulsion concepts for modern airships. *Open Engineering*, 2012, **2**, (2), pp 189-200.
4. LIU, P., DUAN, Z. and MA, L. Aerodynamics properties and design method of high efficiency-light propeller of stratospheric airships. International Conference on Remote Sensing, Environment and Transportation Engineering (RSETE), 24-26 June 2011, pp 8041-8044.
5. TANG, Z., LIU, P., CHEN, Y. and GUO, H. Experimental study of counter-rotating propellers for high-altitude airships. *J Propulsion and Power*, 2015, **31**, (5), pp 1491-1496.
6. NIE, Y. The Design and Experiments Study on High Efficient Propeller Used for Stratospheric Airship (Chinese). MS thesis, 2008, Center for Space Science and Applied Research, Graduate University of Chinese Academy of Sciences, Beijing, China.
7. KOCH, L.D. Design and Performance Calculations of a Propeller for Very High Altitude Flight. MS thesis, 1998 Case Western Reserve University, Cleveland, Ohio, US.
8. MA, R. and LIU, P. Numerical simulation of low-Reynolds-number and high-lift airfoil S1223. *Proceedings of the World Congress on Engineering*, Vol. **2**. 2009.
9. D'ANGELO, S., BERARDI, F. and MINISCI, E. Aerodynamic performances of propellers with parametric considerations on the optimal design. *Calculus of Variations*, 2002, **4**, (5), p 6.
10. LERBS, H.W. Moderately loaded propeller theory. *Transaction of the Soc Naval Architects and Marine Engineers*, 1952, **8**, p 845.
11. CONEY, W.B. A Method for the Design of a Class of Optimum Marine Propulsors. PhD dissertation, 1989, Massachusetts Institute of Technology, Cambridge, Massachusetts, US.

https://doi.org/10.1017/aer.2016.112 Published online by Cambridge University Press

12. EPPS, B., CHALFANT, J., KIMBALL, R., TECHET, A. and CHRYSSOSTOMIDIS, C. OpenProp: An open-source parametric design and analysis tool for propellers, Proceedings of the 2009 Grand Challenges in Modeling & Simulation Conference. Society for Modeling & Simulation International, 2009, pp 104-111.
13. EPPS, B.P. and KIMBALL, R.W. Unified rotor lifting line theory. *J Ship Research*, 2013, **57**, (4), pp 181-201.
14. WRENCH, J.W. The Calculation of Propeller Induction Factors AML Problem 69-54, No. DTMB-1116, Applied Mathematics Laboratory, 1951, David Taylor Model Basin, Washington, D.C., US.
15. BASAVARAJ, A. Estimation of wave drag of non-transonic airfoils using Korn equation. *Int J Innovative Research in Science, Engineering and Technology*, April 2015, **4**, pp 2119-2126.
16. FLUENT Software Package, Ver 6.3.26, Fluent Inc., 2006.
17. SPALART, P.R. and ALLMARCHAS, S.R. A One-Equation Turbulence Model for Aerodynamic Flows, AIAA Paper 92-0439, 1992.
18. MORGADO, J., ABDOLLAHZADEH, M., SILVESTRE, M.A. and PÁSCOA, J.C. High altitude propeller design and analysis. *Aerospace Science and Technology*, 30 September 2015, **45**, pp 398-407.
19. ANDERSON, J.D. *A History of Aerodynamics and its Impact on Flying Machines[M], Appendix G*, 1999, Cambridge University Press, Cambridge, UK.
20. FELLI, M., CAMUSSI, R. and DI FELICE, F. Mechanisms of evolution of the propeller wake in the transition and far fields. *J Fluid Mechanics*, 10 September 2011, **682**, pp 5-3.
21. Heliciel.com, Optimizing the speed and number of blades of the propeller or turbine to capture energy, http://www.heliciel.com/en//logiciel-calcul-helice-aile/optimisation%20vitesse%20rotation%20nombre%20pales%20helice.htm.
22. TREJO, I., TERCEÑO, M., VALLE, J., IRANZO, A. and DOMINGO, J. Analysis of a ship propeller using CFD codes. Calculation of the resistance and the wave profile of a 3600 TEU container ship, 2007.

https://doi.org/10.1017/aer.2016.112 Published online by Cambridge University Press